Inter-areal coupling for cognition through coincident oscillatory transients

Marcus Siems[1]*, Yinan Cao[1], Tobias H. Donner[1], Konstantinos Tsetsos[1,2+], & Andreas K. Engel[1+]

[1] Department of Neurophysiology and Pathophysiology, University Medical Center Hamburg-Eppendorf, Hamburg, Germany

[2] School of Psychological Science, University of Bristol, Bristol, United Kingdom

* Corresponding author

[+] Contributed equally

Contact Information

Correspondence: m.siems@uke.de

Summary

How do large-scale brain networks interact to enable cognition? Correlated oscillations, a mechanism for inter-areal interactions, can be expressed as phase coherence or amplitude co-fluctuations. While considerable work has investigated the functional roles of phase coherence, little is known about whether and how the coincidence of high-amplitude oscillations across the cortex can impact cognition. Here, we demonstrate that inter-areal amplitude-coupling related to cognitive dynamics mainly reflects coincident oscillatory transients, rather than sustained oscillations. Capitalizing on the spatio-temporal resolution of brain-wide magnetoencephalography (MEG) during a behavioral task probing attention and decision-making our findings reveal behaviorally relevant transient oscillatory networks: First, coincidences of oscillatory transients in the alpha and beta frequency range increase prior to correct decisions in a parieto-frontal network. Second, during attention allocation coincident oscillatory transients increase in visual, medial parietal and lateral prefrontal networks in the theta/alpha frequency range. We propose that brain-wide coincident oscillatory events are a key signature of inter-areal interactions during cognition.

Introduction

Cognition requires the exchange of information represented in distant areas of the brain. Neural oscillations index excitability synchronization of local neuronal assemblies[1,2]. Correlations between these local oscillations have been proposed to facilitate the flexible reconfiguration of brain networks to meet the cognitive and behavioral demands of a dynamic environment[1,3–6]. The primary coupling modes associated with large-scale interaction of neuronal populations are phase coupling and amplitude coupling[3,4,7–9]. Phase coupling describes the coherent phase-alignment of frequency-specific population activity[5,10]. Amplitude coupling is defined as the temporal co-modulation of the amplitude, i.e., strength or power, between distant signals[8,11]. Both coupling modes may not only result from but also interact and foster neuronal interactions[4,5].

There is an important gap in the current understanding of these brain-wide correlation patterns. A growing body of literature demonstrates that phase coupling, physiologically constrained through conduction delays, might enable or disable communication by aligning local excitability fluctuations and (oscillatory) spiking input with millisecond precision[5,6,9,10] and modulate in a task-specific manner during cognition[10,12–17] and perception[18–20]. However, the mechanisms underlying neuronal information channels mirrored in amplitude co-fluctuations are not well understood. What has been shown in recent years is that time-averaged amplitude coupling networks are linked to perception[19], memory[21], and decision-making[22] and dissociated from phase coupling in task[23,24], rest[8] and disease[25]. Further, the coupling mode is dynamically modulated at low frequencies (< 0.1 Hz)[11,26,27], influenced by neuromodulatory systems[28] but also displays high-amplitude transient activity[29]. However, what dynamic features of large-scale activity co-fluctuations can aid efficient cognition and behavior?

Recent studies resolving coupling modes dynamically over time[30] can help to elucidate the role of amplitude co-fluctuations in cognition. A growing body of literature has shown that transient high-amplitude events interfuse sustained bandlimited neuronal activity and could aid

inter-areal amplitude coupling and communication[9,17,29,31–35]. Due to time-varying event-rates, transient high-amplitude activity can be mistaken for sustained activity when averaged over multiple trials during task performance[32–34]. Importantly, not every event is the same and high-amplitude events can originate from both, oscillatory or aperiodic transients[9,34,36]. High-amplitude oscillations[29,37,38] reflect rhythmic excitability fluctuations, can result from synchronization in neuronal populations without firing rate modulation, and display narrow-band spectral power increases[17,39,40]. On the other hand, broadband (aperiodic) activity, another meaningful feature of healthy brain function and modulated during cognition[40–42], is linked to time varying firing rate fluctuations[9,43] that, too, can display transient increases in filtered neuronal activity[36,37,40]. Taken together, transiently strong oscillatory- and aperiodic- as well as sustained low-amplitude activity provide potentially distinct information channels and time-scales for neuronal interactions[9,28,43,44]. Thus, if amplitude coupling reflects distinct mechanisms (synchronization vs. firing rate changes), dissociating sustained from oscillatory and aperiodic transient events should reveal distinct networks with dissociable relations to behavior.

Here, we hypothesized that coinciding high-amplitude events, i.e., oscillatory and aperiodic[9,43], enable the rapid reconfiguration of cortical networks required for flexible behavior. To test this hypothesis, we leveraged spatio-temporally precise magnetoencephalography (MEG) recordings with whole-brain coverage to comprehensively unravel sustained and transient components of cortical activity during a challenging cognitive task[45]. Specifically, we utilized transient high-amplitude events coinciding in distant areas to define functional networks and contrast our findings to sustained amplitude co-fluctuations. Assessing time-resolved signal rhythmicity[30,37] enabled us hereby to separate oscillatory and aperiodic high-amplitude event-subtypes.

We found that predominantly coincident oscillatory high-amplitude events, but not sustained network activity, displayed behavioral relevance for decision-making and were modulated during attention allocation. Moreover, brain-wide oscillatory event coincidence network

activity replicated time-averaged functional networks previously observed with amplitude co-fluctuations[8,11]. Overall, our findings demonstrate that for efficient cognition and behavior cortical network activity can be dynamically regulated through transient high-amplitude oscillations. We, thus, propose that coincident oscillatory events are a key signature of large-scale cortical interactions during cognition.

Results

We recorded magnetoencephalography (MEG) from twenty participants (9 female, age_{mean} = 28.05 years ± age_{STD} 4.6 years) to non-invasively assess high-amplitude events in the healthy human brain. During the recording the participants performed a challenging three-alternative decision-making task comparing the contrast of three Gabor patches ($median_{accuracy}$ = 77%, $range_{accuracy}$ = 66–86%) presented at different peripheral locations equidistant from fixation (for details on the task see here[45]).

Recent findings have outlined high-amplitude events as a strong influence on neuronal communication in electrophysiology[17,35]. We thus harnessed (oscillatory) events to directly establish functional coupling, reflected in temporal coincidence of high-amplitude activity in distant cortical sources. In the following we will refer to functional coupling based on oscillatory high-amplitude event coincidences as oECs. We here applied the analyses of event coincidences and of amplitude coupling to pairwise orthogonalized signals to discount spurious coupling due to volume conduction[8,11].

To define coupling via coinciding events, we applied oscillatory and aperiodic high-amplitude event detection using instantaneous frequency stability on source-reconstructed cortical activity over a broad range of frequencies (2–64 Hz; see Supplementary Text 1, Supplementary Fig. S1 and Methods). We validated this approach in three complementary ways. First, we showed that local high-amplitude oscillatory event-rates overlapped well with previously reported[46] cortical generators of oscillatory activity (see Supplementary Text 2 and Supplementary Fig. S2-S4). Second, we demonstrated that time-averaged networks of amplitude coupling components were reliable and, particularly, that transient oscillatory networks predicted previously reported amplitude coupling features (See Supplementary Text 3 and Supplementary Fig. S5-S9). Third, we established that amplitude coupling network components were reliably and

dynamically modulated during the task (Supplementary Text 3 and Supplementary Fig. S10-S13). We then moved on to relate the different coupling measures to different aspects of cognition.

Beta frequency transient oscillatory network activity increases prior to correct decisions

We found that high-amplitude oscillatory event coincidence networks were dynamically modulated during a cognitively demanding decision-making task[45] (Supplementary Text 4). Yet, can the dynamics of transient amplitude co-fluctuation networks predict decision behavior (Fig. 1)? In a first step, we compared oEC dynamics between correct and error trials, matching the number of included (correct and error) trials by experimental conditions to discount effects of task difficulty and sensory salience (see Methods). Averaging over all significant connections ($n_{connection}$ = 104,196) and time points (4.5 seconds time window, n_{sample} = 1,800; paired t-test(19) between oEC in correct and error trials, $p<0.05$) we identified coupling increases during correct trials in the high alpha to beta frequency range (10–23 Hz) with a peak in the low-beta range at 16 Hz (Fig. 1a). We thus focused our initial analysis of performance related coupling on the beta range at 16 Hz. oEC rates increased particularly in the mid-decision phase around 1–2 seconds post-framing and right after stimulus offset (Fig. 1b). Correct choices were associated with coupling increases in a stable network of medial and lateral parietal, posterior temporal and lateral prefrontal areas (Fig. 1c), which appeared to be regulated over the decision phase without apparent network transitions (Fig. 1d).

Further, we identified a smaller subset of oEC connections that were relatively increased during error trials. We identified these connections predominantly in early visual and anterior temporal areas and mainly during the sensory and the early decision phase (Fig. 1b,c).

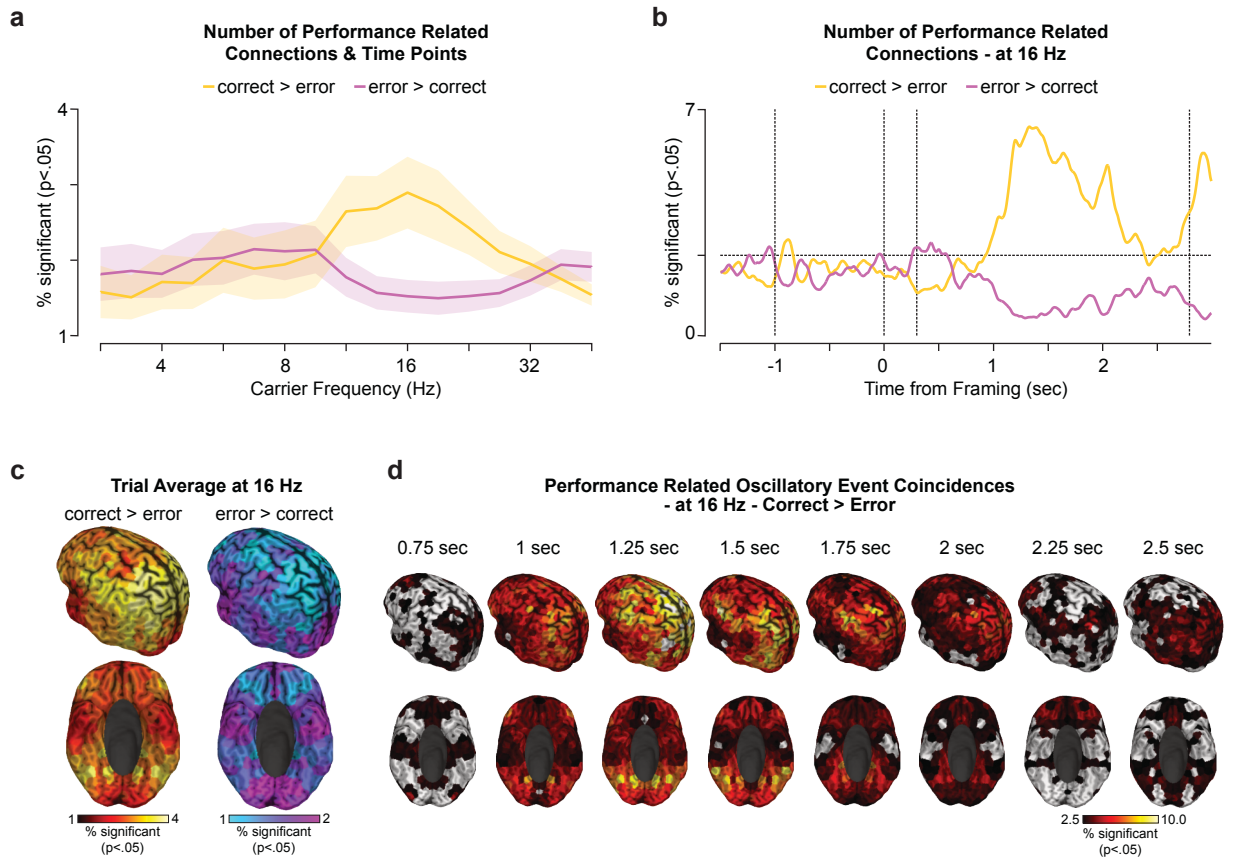

Figure 1 | Oscillatory event coincidence rate at 16 Hz increases prior to correct decisions. a Spectrum of the total number of performance related (correct vs. error, two-sided paired t-test(19), uncorrected p<.05) connections per cortical source averaged over the full trial length (-1.5–2.95 s with respect to the framing cue). Orange and purple lines indicate whether oEC was increased during correct and error trials, respectively. Lines and shaded areas indicate the mean and standard deviation over cortical sources. **b** Time course of the total number of performance related connections at 16 Hz (two-sided paired t-test(19), uncorrected p<.05; color coded as above). Vertical dashed lines denote the stimulus onset, framing cue on- and offset and the stimulus offset (from left to right). **c-d** Cortical distribution of the number of performance related connections per source averaged **c** over the full trial and **d** 0.5 s windows for correct > error (two-sided paired t-test(19), uncorrected p<.05). **d** Timing labels denote each window's starting time with respect to the framing cue onset. The color-scale displays the number of significantly increased (correct > error) oEC connections per time window. The results were averaged over hemispheres.

These findings showed that transiently increased oscillatory network activity can be predictive of behavior. Particularly, beta band coupling during the mid- and late stages of the trial

increased during correct but not error trials. An extended network of behaviorally relevant coupling hereby spanned the medial- and lateral parietal as well as lateral prefrontal areas and the temporo-parietal junction. This network appeared to be stable over time and was quantitatively up-/down-regulated throughout the decision phase.

Dissociating transient and sustained beta frequency amplitude coupling networks in decision-making

Our findings showcased that coincident high-amplitude oscillatory events in the beta range might be used to predict overt behavior in a complex decision-making task. We continued to quantify the behavioral relevance of oECs over the full spectrum. Further, we want to answer the question if partitioning amplitude coupling into transient (oscillatory and aperiodic high-amplitude) and sustained (event free) activity can unravel distinct functional networks. Are there temporally, spectrally or spatially unique features of decision-related network properties that can be attributed to transient oscillatory event coincidences?

In the spectral domain we found widespread performance modulated oEC increases (correct > error) in the beta range (Fig. 2a) and less pronounced decreases (error > correct) peaking in the delta, alpha and gamma frequency ranges (Fig. 1a and Supplementary Fig. S14). Temporally, oEC increases occurred predominantly during the mid- and late decision phase (1–2.5 s from framing). On the other hand, oEC decreases peaked right after framing cue offset between 0.3 to 1 second post-framing. Spatially, the grand average of oEC network changes (Fig. 2b) overlapped strongly with the network identified at 16 Hz alone (Fig. 1). Yet, within each frequency we identified dissociable networks reflecting performance (Supplementary Fig. S15): Up to 8 Hz oECs increased in lateral parietal and lateral prefrontal areas. At 11 Hz we observed an extended parietal and posterior temporal network, while at 22 Hz oECs increased in medial parietal and lateral prefrontal areas. Performance related oEC decreases were generally less pronounced (Supplementary Fig. S14 and S16).

Next, we compared these findings to performance related (correct versus error) amplitude coupling modulations with (Supplementary Fig. S15-S17) and without high-amplitude events (Fig. 2c,d). We found fewer and spectrally as well as spatially distinct performance related connections using sustained (event-free) amplitude coupling. Spectrally, sustained amplitude coupling decreased (error > correct) over the entire trial period in lower frequencies in the delta, theta and alpha range up to 8 Hz (Supplementary Fig. S14). Spatially, performance modulated increases (correct > error) emphasized a fronto-parietal and early visual network and decreases in a medial parietal, medial peri-central and ventral frontal network (Supplementary Fig. S15). Hereby, the cortical distribution of performance related sustained amplitude coupling appeared to be stable over frequencies yet most pronounced in the high alpha to beta range (8–23 Hz; Supplementary Fig. S15).

Transient aperiodic event coincidences displayed performance related changes (correct > error) in a parietal, temporal and ventral stream visual network spatially overlapping with identified transient oscillatory network changes (compare Fig. 2b and Supplementary Fig. S18). However, transient aperiodic network changes were spectrally constrained to high frequencies in the high-beta to gamma range and to time points around stimulus offset.

Our results further indicated that amplitude coupling (including events) effects related to performance appeared to be a mixture of transient oscillatory network activity and sustained amplitude coupling (Supplementary Fig. S15-S17). We systematically correlated the behavioral effects, both in time and over the cortex. We found that oEC and effects of event-free amplitude coupling shared little overlap below the gamma frequency range (Fig. 2e,f ; $R^2_{cortex,2.8\text{-}27Hz}$ = [<0.01, 0.54], $R^2_{time,2.8\text{-}27Hz}$ = [<0.01, 0.13]). Furthermore, amplitude coupling effects (including events) could to large extends be explained through oECs for frequencies up to the beta ranges ($R^2_{cortex,2.8\text{-}23Hz}$ = [0.25, 0.71], $R^2_{time,2.8\text{-}23Hz}$ = [0.34, 0.95]). Yet, amplitude coupling (including events) overlapped with sustained low-amplitude coupling at higher frequencies (Supplementary Fig. S15e,f; $R^2_{cortex,27\text{-}45Hz}$ = [0.72, 0.97], $R^2_{time,27\text{-}45Hz}$ = [0.89, 0.99]).

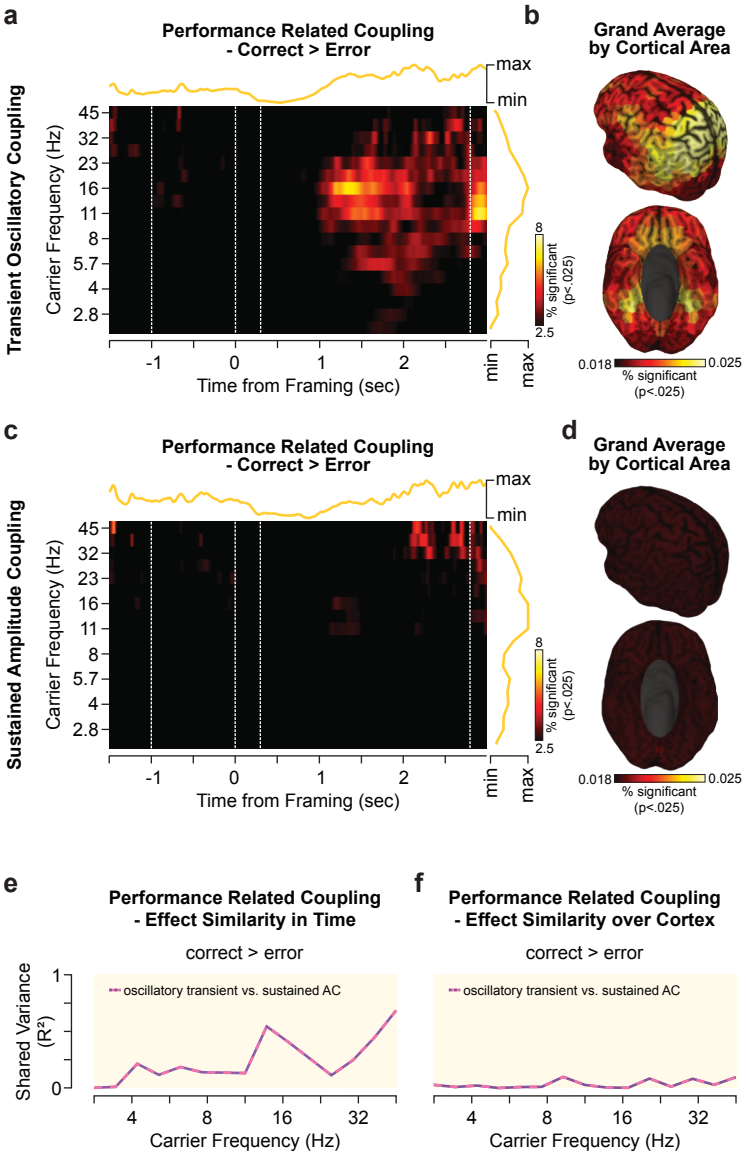

Figure 2 | Spectral and spatial dissociation of performance related amplitude coupling networks. a Time and frequency resolved distribution of performance related (correct > error, one-sided t-test(19), uncorrected p<.025) transient oscillatory amplitude coupling connections. Colored lines on top and to the right denote the average over frequencies and time, respectively. **b** Average over the full time and frequency resolved distribution of performance related oscillatory event coincidence modulations within each cortical source. **c-d** Same as **a-b** for sustained (event-free) amplitude coupling. **e-f** Pearson correlation of the behavioral coupling effects between transient oscillatory and

sustained amplitude coupling (AC) comparing the **e** temporal (see Fig. 2a,c) and **f** spatial (Supplementary Fig. S15) distribution of effects. The values depict the shared variance (R^2) within each frequency.

All in all, transient high-amplitude oscillatory networks were modulated up to 1.5 seconds before a correct choice was made. Coincident high-amplitude oscillatory event rates increased particularly in the alpha and beta range (8–23 Hz) when participants made a correct choice. Our findings further demonstrate that decision-related functional networks dissociated temporally, spatially, spectrally and in magnitude between transient (events) and sustained (event-free) amplitude coupling modes. Consequently, particularly transient amplitude coupling components might echo large-scale interactions related to decision behavior.

Coincident transient theta/alpha oscillations govern network dynamics during attention allocation

Our analyses described above show that transient and sustained components of dynamic amplitude coupling uncover distinct functional networks associated with behavioral performance in decision-making. We next studied the relation of these coupling patterns to another domain of cognitive dynamics: the spontaneous allocation of selective visual attention[47]. In a previous study[45] we showed that we can decode the momentary focus of attention and track brief changes of covert visual-spatial attention[45,48], that can occur at any time during the trial. Covert attention strength intrinsically fluctuated around 9–12 Hz with attention reallocating between (switch) and refocusing on the same (stay) decision alternative at the trough and the peak of this oscillation, respectively[45].

Here, we ask if transient (oscillatory) and sustained amplitude coupling components were modulated differently during attention allocation. In a first step, we quantified attention-triggered oECs at 10 Hz separately around attention reallocation and refocus onset (Fig. 3a). When averaging over all connections we found a significant increase (two-sided, paired t-test(19),

$p_{FDR}<0.05$) of oECs during attention reallocation compared to refocusing (switch vs. stay; see also Supplementary Fig. S19 for associated resting-state networks).

Next, we systematically assessed attention-related coincident oscillatory event rates over the entire spectrum and identified coupling modulations not only in the alpha but also the theta and beta frequency ranges (Fig. 3b). On average over the cortex, between 9% (theta, 6 Hz) and 11% (alpha, 10 Hz) of all connections displayed increased transient oscillatory coupling right around attention reallocation between alternatives (switch; per connection: paired t-test(19) of average oEC rate (-0.05–0.05 s from event), switch vs. stay, uncorrected $p<0.05$). Hereby, switch-related oECs were broadly increased peaking within the theta and alpha frequency range (Supplementary Fig. S20-S22) highlighting a network including ventral stream and early visual as well as medial parietal and lateral prefrontal areas (Fig. 3c). We identified fewer stay-related coupling changes (Fig. 3c and Supplementary Fig. S22). Transient aperiodic networks did not display a compatible modulation with attention (Supplementary Fig. S23).

However, a very different coupling-to-cognition relationship emerged for sustained amplitude coupling (Fig. 3d-f). While amplitude coupling including high-amplitude events mirrored our findings of attention-modulated transient oscillatory coupling spectrally and spatially (Supplementary Fig. S21), we found marked changes when excluding all transients. First, coupling within a lateral parietal and lateral prefrontal network was increased during reallocation (Fig. 3f) but we did not find an attention modulation of coupling within other attention networks or for the connection average (Fig. 3d and Supplementary Fig. S19b). Generally, over the entire spectrum attention modulated fewer sustained amplitude coupling connections (Fig. 3e; compare to Fig. 3b; see also Supplementary Fig. S20-S22). Again, the smaller effect cannot be readily explained by weaker reliability (Supplementary Fig. S8) or statistical power. Further, we directly compared the attention-modulation effects between coupling components (Fig. 3g-i), i.e., correlation of frequency specific cortical distributions of attention modulation (see Supplementary Fig. S20 and S21). We found the highest correlation between oECs and amplitude coupling

(including events; Fig. 3h) for frequencies below 32 Hz for attention reallocation networks (switch; $r_{switch,2.8\text{-}32Hz}$ = [0.62, 0.80]) and a high effect correlation between standard and sustained (event-free) amplitude coupling (Fig. 3i) at higher frequencies ($r_{switch,19\text{-}45Hz}$ = [0.62, 0.88]; $r_{stay,19\text{-}45Hz}$ = [0.50, 0.90]). Lastly, oECs and sustained amplitude coupling effects displayed weaker correlations over the entire spectrum only exceeding |r| > 0.3 in the beta range ($r_{switch,16\text{-}27Hz}$ = [0.38, 0.65]; Fig. 3g).

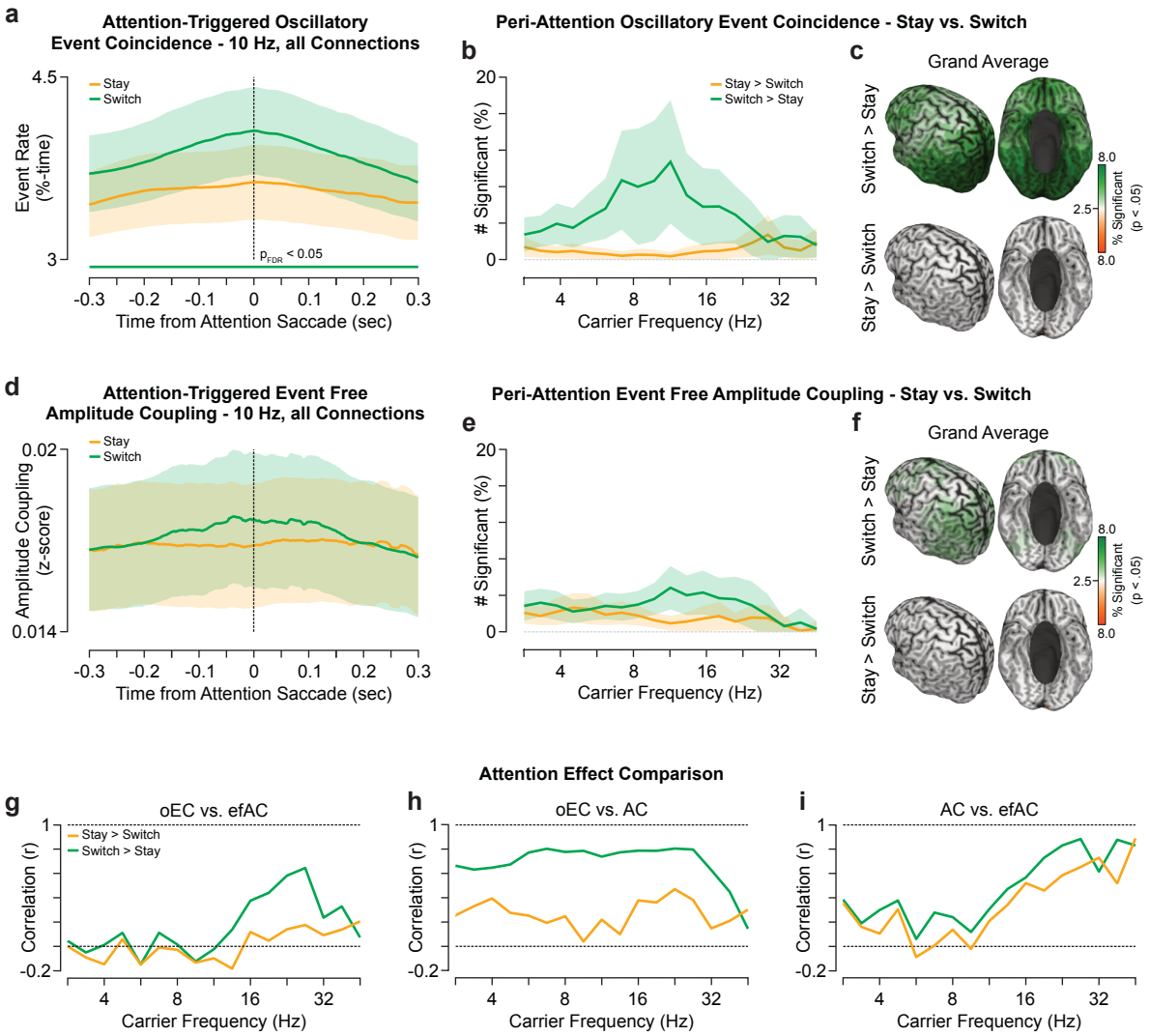

Figure 4 | Amplitude coupling components dissociate during attention reallocation. a Attention-triggered oscillatory event coincidences (oEC) at 10 Hz separately for attention reallocation (switch, green) and refocus (stay, orange) averaged over all connections. Colored lines and shaded areas denote the mean and standard deviation over

participants (n = 20). Thick lines denote the time of significant difference between switch and stay (two-sided paired t-test(19), p_{FDR}<.05, FDR-corrected over time). **b** Number oEC connections modulated by attention (paired two-sided t-test(19), uncorrected p<.05) at the time of attention allocation (averaged between -0.05 to 0.05 s) spectrally resolved between 2.8–45 Hz. Green and orange lines denote the mean proportion of connections per source increased during attention reallocation (switch) and refocusing (stay), respectively. Shaded areas denote the standard deviation over cortical sources. **c** Grand average of the proportion of attention modulated oEC connections from each cortical source averaged over all frequencies. **d-f** The same as **a-c** for sustained (event-free) amplitude coupling. **g-i** Correlation of attention modulation effects between coupling measures. The correlations were computed between frequency-specific cortical distributions of the number of switch- and stay-modulated connections (see Supplementary Fig. S21 and S22) for **g** oEC against event-free amplitude coupling (efAC), **h** oEC against full amplitude coupling including events (AC), and **i** between efAC and AC. Color-coded as above.

All in all, our result showcased that attention reallocation modulated transient oscillatory amplitude coupling. Transient oscillatory event coincidences were amplified in an extended visual, medial parietal and lateral prefrontal network predominantly in the theta and alpha frequency range at the moment of attention reallocation. The coupling effects for attention refocusing were generally weaker. Further, by excluding high-amplitude events, sustained amplitude coupling displayed little attentional modulation. These findings further underline the functional, spatial and spectral dissociation between transient and sustained neuronal dynamics and their putative roles in large-scale cortical interactions during cognition.

Discussion

The exchange and integration of information over long distances within the brain is a prerequisite of flexible cognitive processing. Precise temporal relationships of neuronal activity, i.e., phase coupling, between distant areas has been associated with fostering and parsing this communication. However, little has been known about the functional role of co-fluctuations of local activity, i.e., amplitude coupling, in cognition and long-range communication. Leveraging the rich spatio-temporal resolution of non-invasive electrophysiological measurements we here demonstrated that transient oscillatory dynamics are a central hallmark of large-scale neuronal interactions. We established that brief events of high-amplitude oscillatory activity govern the network architecture during cognition. Hereby, high-amplitude oscillatory network activity was relevant to decision behavior, indicative of better performance. Further, networks of coincident oscillatory events were transiently modulated during attention allocation. Sustained low-amplitude co-fluctuations, on the other hand, showed a weaker modulation with cognition while displaying compatible reliability. Moreover, the associated networks supporting cognition were spatially and spectrally distinct between sustained and transient oscillatory coupling components. We, thus, argue that not only sustained activity but particularly the orchestration of transient oscillatiory events can facilitate inter-areal coupling and efficient cognition. We thus provide a framework integrating dynamic large-scale amplitude co-fluctuations into distinct neuronal circuit mechanisms.

Within this framework we understand local activity and long-range co-fluctuations of signal strength, i.e., amplitude coupling, as resulting from a composite of at least three non-exclusive circuit-level mechanisms: Neuronal synchronization, (aperiodic) firing rate modulations and neuromodulatory excitability fluctuations[1,5,9,28,44]. Neuronal synchronization refers to local excitability fluctuations temporally ‘biasing’ neuronal spiking and resulting in (oscillatory) narrow-band frequency peaks of large-scale electrophysiology[1,3,7,40,41]. Temporally less constrained firing

rate modulations can result in high-frequency activity (80–200 Hz)[49] of large-scale recordings and broadband power shifts in lower frequency ranges[28,40–43]. Lastly, neuromodulatory systems can alter local excitability and the neuronal firing readiness[28]. The first two of these three mechanisms can further affect local activity on very short time scales and might lead to the detection of high-amplitude events[9,32–34,36]. Here, we argue that large-scale oscillatory and aperiodic events, identified and dissociated through signal rhythmicity[30,37], can serve as a handle for studying the functional relevance of these circuit-level mechanisms. Our findings present a falsifiable testing ground for studies invasively assessing or causally modulating local activity as well as long-range interactions. Further research is thus needed to directly link oscillatory and aperiodic transients as well as sustained low-amplitude activity to neuronal firing rate fluctuations and interactions.

Moreover, coinciding oscillatory events provide a physiological link between local population activity and large-scale amplitude coupling. As local activity oscillates[1,3,7,40], amplitude coupling has been proposed to indicate the co-regulation of local excitability fluctuations between distant areas[3,4,9,43]. Our results support this view empirically. Importantly, apart from sustained oscillations we found that the co-occurrence of high-amplitude events, both oscillatory and aperiodic, demonstrated dissociable coupling and thus potentially distinct communication channels. Particularly brain-wide coupling of transient oscillatory events demonstrated (i) to be a reliable measure for functional networks (Supplementary Fig. S6), (ii) well explained previously reported amplitude coupling networks[8,11] while dissociating from sustained (event free) coupling from the delta up to the beta frequency range (Supplementary Fig. S6), and (iii) accorded for independent insights into cortical interactions during cognition (Fig. 2 and 3). Overall, our results, thus, present amplitude co-fluctuations as an intrinsic coupling mode that might capture predominantly synchronized neuronal firing but also transient and sustained firing rate fluctuations.

Disentangling different components of amplitude coupling can further help to directly address theories of large-cale neuronal communication. When local oscillatoryevents coincide

across distant brain regions they also represent periods of heightened coherent activity[5,6,9,29,31]. With respect to for example the 'Communication through Coherence' (CTC) model of large-scale interactions these periods are central to enabling/disabling direct information exchange[14,49] with computational models highlighting strong oscillatory activity as a prerequisite for CTC[6]. Thus, the inter-areal phase relationship during transient oscillatory events might be informative for effective communication and behavior[5,13,47,49]. Further, within our framework we can empirically dissociate the CTC model from competing information channels: 'Coherence through Communication' (CTC*) and 'Communication through Resonance' (CTR)[9]. Here, CTC* refers to pseudo-interactions between neuronal populations that occur through correlated output of the sending area with its own input to the receiving area. In contrast to CTC, here, the inter-areal phase-difference would be fixed via conduction delays and ion-channel time constants. In CTR, due to intrinsic structural properties of the receiving population, certain input frequencies elicit stronger responses, i.e., resonance. Consequently, the instantaneous frequency of the sending units might show high variability, i.e., low rhythmicity, prior to connecting, indicating a transition towards a resonance frequency[9]. Overall, it appears pivotal to further assess the relationship of different amplitude coupling components and phase coupling to understand their roles in flexible information routing[5,9,17,35].

Another central finding has been that cognition and behaviorally-altered functional coupling displayed spatially and spectrally dissociable networks between transient and sustained signal components that might represent distinct cognitive functions. First, during correct choices in a difficult three-alternative decision-making task sustained amplitude coupling highlighted the lateral parietal and medial prefrontal cortex associated with integrative functions as for example error monitoring and evidence accumulation[50]. On the other hand, transient oscillatory coupling displayed an increase between the medial, posterior parietal and lateral prefrontal areas, i.e., areas associated with output preparation and comparing sensory evidence[51]. Second, transiently coinciding oscillations were the coupling component to best represent brief attention reallocation

(Fig 3), i.e., attentional saccades[48]. In the theta (5–6 Hz) and high alpha (9–11 Hz) frequency range a network of early visual, posterior parietal and lateral frontal areas was modulated during attention reallocation[45,48]. While keeping the focus of attention (refocus) was more strongly associated with sustained amplitude coupling in prefrontal areas (Fig. 3 and Supplementary Fig. S20). In sum, all our findings provide initial evidence that cognitive processes relying on either information integration or change detection might consequently form communication channels utilizing either sustained or transient amplitude dynamics, respectively. The functional role of large-scale communication channels might thus depend on both, intrinsic and endogenous time scales of cognition.

Establishing non-invasive markers for intrinsic large-scale interactions, as outlined in the current study, is a pivotal requirement to study healthy and atypical neuronal communication at scale. Yet, there are limitations to the presented results that can be addressed in future research. First, our framework relies on a correlative link between cognition, (oscillatory) signal strength dynamics and circuit-level mechanisms. As we have pointed out above the direct link between the meso- and the macro-scale of neuronal activity needs to be investigated directly. Second, pharmacological interventions might further explicate this relationship non-invasively. Critical dynamics, arousal and the balance between excitatory and inhibitory neural activity have been shown to influence oscillatory and aperiodic processes[28,37,40–42]. Pharmacological alterations of the excitation/inhibition ratio for example have quantifiable effects on local and inter-areal oscillatory and aperiodic activity in health[28,42]. Third, we can then leverage these pharmacological agents to elucidate malfunctioning coupling in the diseased brain. Lastly, we can apply electrical stimulation to identify causal links between neuronal coupling and cognition[4]. For example, amplitude-modulated transcranial alternating-current stimulation (AM-tACS) puts forward an approach to directly test transient oscillatory network activity. The principle of AM-tACS is to electrically stimulate neuronal tissue with a sinusoidal carrier frequency that is modulated in

strength over time. It is thus by definition an oscillatory process that can display transiently enhanced activity at stimulation peaks[52].

In sum, our study showed that amplitude coupling is a dynamically rich intrinsic coupling mode that is dominated by the coincidence of transiently high oscillations. By identifying high-amplitude oscillatory events coinciding over the cortex we could reliably explain previously reported amplitude coupling networks in the delta, theta, alpha and beta frequency ranges with only a fraction of the data. Importantly, we highlighted that not every high-amplitude event is oscillatory and that transient aperiodic activity might itself be a distinct feature of neuronal communication. Additionally, sustained amplitude coupling displayed reliable yet dissociable network features. Averaging neuronal activity and functional coupling over extended time periods might thus lump together various informative and dissociable processes. Particularly during cognition sustained and transient coupling components might cater to qualitatively distinct functions and information processing time scales. Our results highlight that efficient cognition and behavior might rely on information channels forming through co-occurring transient oscillations. We, thus, propose that networks of coincident oscillatory events are a key signature of inter-areal interactions during cognition.

Methods

Participants and experimental procedure

Participants. The task and participant group has been described in detail in[45]. In short, we tested twenty right-handed participants (9 female, age_{mean} = 28.05 years ± age_{STD} 4.6 years) in a decision-making task. The experiment was approved by the ethics committee of the Hamburg Medical Association and conducted in accordance with the Declaration of Helsinki. All participants gave their written informed consent and received monetary compensation for their participation.

Decision-Making Task. The main task was a three-alternative forced-choice protracted decision-making task with variable task framing. During central fixation three peripheral Gabor patches (2.2° eccentricity, 1.6° stimulus diameter) of varying contrast levels and orientations appeared simultaneously on screen (at the top and 120° left and right of it). The three stimuli were drawn from a set of five linearly spaced contrast levels (10 possible combinations, i.e., stimulus conditions). We used for each participant a staircase procedure to find the threshold physical distance between neighboring contrast levels and to control the task difficulty. The Gabor patch orientations were drawn from a set of three equally distant orientations with either all three being identical or different and pooled our analyses over orientation conditions. We did not utilize the orientation feature in the presented analyses.

Each trial started with the presentation of the central fixation cross. Participants were instructed to keep fixation and blink as little as possible during the trial. After 1 second the three Gabor patches appeared on screen and remained unaltered for 3.8 seconds. The task framing, i.e., if participants had to choose the highest ("Hig") or lowest ("Low") contrast, was centrally cued between 1–1.3 seconds into the stimulus presentation and randomized between trials. The high contrast stimulus represents the highest value in high framing trials, but the lowest value in low framing trials. The task framing divides the stimulus presentation period into the sensory- (pre-framing, -1–0 seconds from framing cue) and decision-phase (post-framing, 0.3–2.8 seconds)

with identical visual stimulation but distinct cognitive demands. After the 3.8 second stimulus presentation, the Gabor patches turned off and the response cue (fixation cross rotated 45°) started the maximum 2 seconds response window. Participants indicated their decision with a left thumb, right thumb or foot button press for the left, right or top alternative, respectively. We randomized the foot (left or right) between participants. We individually adjusted the height and location of the pedal for each participant using Styrofoam such that the position was comfortable and a response could be triggered with a small flexion of the porcellus fori. We gave binary feedback after each trial (fixation cross: green for correct, red incorrect). We fully randomized task framing, contrast levels, Gabor orientation and stimulus locations, yielding 1080 unique trials. Every participant concluded two full randomization runs. We blocked the trials into random 120-trial sets (n_{block} = 18). Participants chose the correct contrast on average in 77% of all trials (range = [66% 86%]). For the analyses comparing decision-making performance (correct vs. error) we matched the trials included for both performance levels by stimulus conditions and framing cue to account for difficulty and salience effects.

Stimulus Localizer Task. Prior to each block of the decision-making task the participants concluded a localizer block: 90 trials of consecutively presented single Gabor stimuli in one of the three locations at full contrast for 0.35 seconds with 0.5 seconds inter-trial intervals. The stimuli matched the decision-making task in size and eccentricity. Participants were instructed to ignore the peripheral stimuli, fixate at the center and detect a flickering of the central fixation cross that could occur randomly at each stimulus. In total, a flicker occurred 9 times per block, and participants indicated the detection with a button press. In each block we fully randomized the orientation and the position over the three locations. Each stimulus combination was repeated ten times paired once with a central fixation flickering. We used the localizer task to decode the visual representations of all three stimuli during the decision-making task.

Functional data acquisition and preprocessing

Data acquisition. During the experiment the participants were sitting upright in a whole-head magnetoencephalography scanner (MEG; 275 axial gradiometer sensors, CTF Systems Inc.) in a magnetically shielded room. The data was acquired at a sampling rate of 1200 Hz. Each participant's head position was tracked online using three head localization coils (nasion, left/right preauricular points). Additionally, we recorded a 2-channel bipolar electro-oculogram (horizontal and vertical EOG) and a single channel bipolar electro-cardiogram (ECG) to control for cardiovascular and ocular signal artifacts. Eye-movements and pupil diameter were tracked using an MEG-compatible Eyelink 1000 system (SR Research). We further collected T1-weighted structural magnetic resonance images (MRI; sagittal MP-RAGE) to reconstruct individualized high-resolution head models.

Preprocessing. The detailed MEG preprocessing pipeline can be found in[45]. We band-pass filtered the continuous MEG data segments between 0.2 and 200 Hz (4th order Butterworth filter) and down-sampled it to 400 Hz. We filtered the line noise with a notch filter at 50 Hz and its first 6 harmonics (1 Hz stop-band filter width). Next, we implemented a two-stage procedure for artifact rejection[53] applying filtering the signal into two distinct frequency ranges (low- from 0.2 to 30 Hz; high-range from 30 to 200 Hz), separately computed independent component analyses on each range and rejected artifact components based on their topology, power-spectra and time-courses[54].

Spectral analysis and source reconstruction

Spectral analysis. We generated time-frequency resolved MEG signals using Morlet's wavelets[53] (wavelet bandwidth at 0.5 octaves; $f/\sigma_f = 5.83$; kernel width covered $\pm 3\sigma_t$; σ_f and σ_t corresponds to standard deviation in frequency and time domain). We derived complex spectral estimates for frequencies between 2 to 90.5 Hz in quarter octave steps (2^1 to $2^{6.5}$ Hz).

Source projection. We generated single-shell boundary-element method models (BEM) based on individual structural MRI. The physical forward model (leadfields) for 457 equally spaced cortical sources (~1.2 cm distance, at 0.7 cm depth below pial surface) was computed using FieldTrip[55].

We applied dynamic imaging of coherent sources (DICS) linear beamforming to estimate the source-level neuronal activity. For seed-based analyses we used cortical source positions in the left auditory cortex (lAC, [-54, -22, 10]), left somatosensory cortex (lSSC, [-42, -26, 54]), medial prefrontal cortex (MPFC, [-3, 39, -2])[8], posterior medial temporal lobe (MT, [±39, -83, 15]), medial parietal cortex ([0, -64, 67]), lateral parietal cortex ([±41, -68, 44]), and lateral prefrontal cortex (PFC, [55, 13, 35]), all part of the source-model and in MNI-coordinates.

Defining transient high-amplitude events

We defined transient high-amplitude events as episodes of bandlimited high-amplitude activity. Here, we z-scored the squared amplitude, i.e., signal power, of the complex time-frequency resolved data over the full experiment within each cortical source. Prior to z-scoring, we subtracted the trial-averaged activity. Within each source and frequency, we recorded high-amplitude events as time points with a z-score larger 3.

Oscillatory vs. aperiodic events. To identify if a sample within a high-amplitude event is oscillatory or not, we leveraged the phase-progression stability of band-limited oscillatory activity[37]. A pure oscillation exhibits a progression through the phase cycle with uniform speed, i.e., a stable instantaneous frequency (see Supplementary Fig. S1). A filtered aperiodic signal on the other hand will display a more variable instantaneous frequency distribution through intrinsic frequency modulation. First, we computed for each time point $\boldsymbol{t}$ and source $\boldsymbol{i}$ the cross-spectrum c between the signal $\boldsymbol{x_t}$ with its past $\boldsymbol{x_{t-1}}$.

$$c_{i,t} = x_t * x'_{t-1}$$

Where $\boldsymbol{x'}$ denotes the complex conjugate of the signal. We then derived the first-order temporal derivative of the instantaneous phase $\boldsymbol{\Delta\varphi}$ as the inverse tangent of the imaginary, divided by the real part of the cross-spectrum[30].

$$\Delta\varphi_{i,t} = \mathrm{atan}\left(\Im(c_{i,t})\,/\mathcal{R}(c_{i,t})\right)$$

The absolute value **||** of the instantaneous phase derivative describes the phase progression stability over time. The instantaneous frequency $f_{i,t}$ can then be derived.

$$f_{i,t} = \left|\Delta\varphi_{i,t}\right| / (2 * pi) * f_{sample}$$

Where f_{sample} denotes the sampling frequency of the signal. Finally, we defined oscillatory time points as neighboring samples displaying the lowest first-order temporal derivative of the instantaneous frequency (IFD), i.e., moments of the most stable phase progression, by thresholding.

$$IFD = \left|\frac{df_i}{dt}\right| / f_{carrier}$$

$$IFD_{t,t+1} \begin{cases} < 0.0025 \in Osc \\ \geq 0.0025 \ \notin Osc \end{cases}$$

In other words, if the instantaneous frequency difference between neighboring samples, ***t*** and ***t+1***, is smaller than 0.25% of the carrier frequency $f_{carrier}$ we considered time point ***t*** to be most likely oscillatory. For a pure sinusoid the IFD will be equal to zero (see Supplementary Fig. S1). Overall, the approach needs only three samples of the signal to generate a proxy of oscillatory activity, i.e., at a sampling rate of 400 Hz only 0.0075 seconds. The threshold parameter was derived as the approximate median 25th percentile of the IFD over the cortex at 11 Hz ($2^{3.5}$ Hz). Thus, at 11 Hz approximately 25% of time points for each source are set to be most likely oscillatory. We selected the alpha range as a reference frequency due to the large body of literature identifying oscillatory alpha activity[37,40,44]. The threshold scales well with carrier frequency because the constructed Morlet wavelets filter widths are adaptive.

Lastly, we defined oscillatory and aperiodic high-amplitude events as co-occurring or not co-occurring with a stable instantaneous frequency, respectively.

Analyzing Event Dynamics

Event rate and duration. We computed the local oscillatory event rate as the percentage of time points that an oscillatory event occurred at a given source and frequency. Under random conditions, i.e., no oscillatory activity, the minimum expected event rate can be derived from

multiplying the probabilities of the signal crossing the amplitude and the IFD threshold (for frequencies: $median_{2\text{-}64Hz}$ = 0.26%, $range_{2\text{-}64Hz}$ = 0.03–0.34%). The relative event rate is the percentage of oscillatory events among all recorded high-amplitude events. Under random conditions the average relative oscillatory event rate would converge towards the probability of crossing the IFD threshold parameter (for frequencies: $median_{2\text{-}64Hz}$ = 29.3%, $range_{2\text{-}64Hz}$ = 2.7–35.2%). We applied fixed thresholds to explicitly address potential differences in the frequency-specific amplitude ($z_{threshold} > 3$) and instantaneous frequency ($\Delta f_{threshold} < 0.25\%$) distributions. The duration describes the median length of each high-amplitude event. Due to adaptive filter width of the applied Morlet wavelets the amplitude modulation can only depict a smaller range for lower frequencies and durations, measured in units of time, will be longer. We thus also computed the duration in units of cycle length by multiplying with the carrier frequency.

Cortical Event Coincidence Definition. As an intermediate step between local events and assessing co-occurrence of events in networks we computed the cortical event coincidence. The measure describes the number of cortical sources displaying high-amplitude events locally for each moment in time and can range between no sources (size = 0) and all sources displaying events (size = 1). We generated the histogram of cortical event coincidences for each frequency and participant in steps of 1/457 (n_{source} = 457). We divided the histogram bins by the integral over the full histogram to generate the probability distribution of event coincidences. Lastly, we computed the exponential decay function of the histogram via fitting a linear model to the log-log scaled histograms between 1/457 and 46/457 (10% cortical size). A steep or shallow slope indicates a lower or higher probability for large cortical coincidence, i.e., widespread occurrence of cortical high-amplitude events.

Functional coupling analyses

Amplitude Coupling. We applied two different approaches to quantify the statistical relationships between the signal strength of distant cortical sources: Amplitude coupling and event coincidences. For the amplitude coupling we pairwise multiplied (dot product) z-scored power

envelope (squared amplitude) signals between a seed and a target region. These seed-target cofluctuations were either averaged over time, yielding the correlation coefficient (tima-averaged coupling analysis) or used to describe the temporal dynamics of amplitude coupling[30]. To discount effects of volume conduction, we orthogonalized the target- onto the seed signal prior to squaring and z-scoring the power envelopes[11]. The z-scoring was conducted over the full dataset within each cortical source and frequency. For the full correlation matrices (source x source) we applied the orthogonalization in both direction with signals x and y as the seed and target and vice versa.

Event Coincidence. We quantified coincidences of oscillatory events between distant cortical sources as the "logical and" operation for the occurrence of high-amplitude events and stable instantaneous frequency in both the seed and target signals at the same time. Aperiodic events on the other hand showed high amplitude without IF stability in both sources. Hereby, the definition of high-amplitude events was based on the same orthogonalized z-scored power envelopes as the amplitude coupling. Coincidence under random conditions was estimated by multiplying the respective local event rates from seed and orthogonalized target, i.e., co-occurring events without temporal relationships between seed and target. The oscillatory (and aperiodic) coincidence time courses thus are binarized signals with zeros and ones indicating no coincidence and coincidence, respectively. Again, averaging these signals over time yields the coincidence rate for a specific connection (time-averaged coupling analysis), while the binary time courses were used to describe dynamic coupling with respect to external and internal events. Additionally, we computed event free amplitude coupling (efAC) by excluding all local event time points from the seed-target power cofluctuations, i.e., we set high-amplitude event time points to nan (not a number).

Data simulation

To highlight the distinct features of oscillatory and aperiodic events we simulated 5 second traces of random data *x* with a pink noise spectrum (power ~ 1/f; $n_{simulation}$ = 100,000). We split each data trace into five 1-second windows (I-V). We multiplied the data in window II by 3 (*3x*) to increase

broadband (aperiodic) power. We further multiplied window IV by 0.8 and added a constant 10 Hz sine wave *y* with an amplitude of 0.8 ($0.8x + 0.8y$), to increase oscillatory activity and bandlimited power. The modulation parameters were chosen to i) approximately match the broadband power between the random data segments (I, III, V) and the sine modulated window IV as well as ii) approximately matching bandlimited power between 8–12 Hz for both modulated windows (II and IV). We estimated the broadband power within each window as the integral of the windowed Fourier transform. We applied the same Morlet wavelet transformation as outlined for the empirical data with a center frequency at 10 Hz and estimated the bandlimited power from the broadband Fourier transform solution between 8–12 Hz. We applied the event detection algorithm on the bandlimited full data trace while z-scoring the data according to the mean and standard deviation from windows I, III, and V for each simulation repetition. The IF stability threshold was set to the 10% percentile over windows I, III, and V.

Encoding the focus of covert attention

We used a stimulus localizer task to reconstruct the competition of stimulus representations during the decision-making task and thereby track the focus and strength of attention. Here, we implemented an inverted encoding model[45]. The encoding model assumes that the sum of abstract neuronal populations, i.e., information channels responsive to a given stimulus angle, is represented in the multivariate sensor-level MEG activity. Activity and tuning for an information channel can thus be estimated as the weighted sum of this MEG activity plus noise. The activity derived from inverting the model for MEG activity in the decision-making task then denotes momentary changes of the visual representations of the simultaneously presented stimuli.

Training Encoding Model. We trained the encoding model on the retinotopic stimulus localizer task. During the localizer task only one stimulus out of the full set has been visible on screen. Hence, during the localizer both neuronal activity and the to be represented visual stimulus were known variables. We used bell-shaped tuning-curves (half-wave rectified sinusoidal) as design matrix to identify a linear weight-matrix relating neuronal activity and the presented stimuli[45]. We

further used multivariate noise normalization on the weight-matrix to address correlated sensor activity, i.e., volume conduction, and improve reliability.

Applying Inverted Model on Task. With the optimized weight-matrix we can estimate the latent visual representation of the stimuli during the multi-alternative decision-making task. We inverted the model, i.e., the weight-matrix, and multiplied the MEG activity during the decision-making task. The solution of this operation yielded the representational activity over visual stimuli for each time point during the task. The strength of the representations is a proxy of covert visual attention towards each target on screen.

Reconstruct Attention Focus. We used the vector sum of the three representational activities as a handle on the attention focus[45]. The vector orientations were set to 0°, 120° and 240° for the top, left and right stimulus, respectively and the representational activity corresponded to the length at each orientation. The reconstructed attentional vector can illustrate two features of visuo-spatial attention: First, the overall attention/alertness[56] paid to the stimuli and second, the main target of information sampling. Thus, we considered the length of the vector as a proxy for overall attention and the direction, i.e., the angular similarity to the three alternatives, as the most likely target of covert spatial attention at each time point. Importantly, this quantification of covert attention cannot be solely explained by fixational eye-movements or (micro-)saccades[45].

Model Training Parameter. We optimized the decoding performance within the localizer task by varying the training time point with respect to stimulus onset. Applying leave-one-block-out cross-validation (n_{block} = 18 per participant) we selected the time-window from 0.14–0.17 seconds after stimulus onset as training epoch[45]. For the model training we excluded stimulus localizer trials displaying (micro-)saccadic activity within the first 0.2 seconds after stimulus onset. On average 3% of all localizer trials per participant (mean = 3.03%, median = 1.82% range = 0.50% - 10.68%) were excluded.

Defining moments of attention reallocation and refocus. We leveraged the temporal dynamics of the attention vector to define moments when attention shifted from one alternative to another. The

momentary focus of spatial attention was assessed via the angular similarity between the attention vector and the vector orientations corresponding to the three stimuli. At every moment the vector can point close to one decision alternative or in between two options. We defined a threshold to identify time points where attention is focused at one alternative as the 90th percentile of the angular similarity distribution[45]. However, the vector is oriented in circular space and will even under random conditions, i.e., without visual stimulation or participant's alertness, point towards one of the three stimuli. We thus applied a second threshold on the vector length (within trial 90th percentile). An attentional saccade is only recorded when both thresholds, i.e., orientation and length of the vector, are crossed at the same time. We only recorded the first sample when both thresholds were crossed and excluded the following 0.025 seconds to not count individual events twice. We previously assessed the effects of different thresholds and concluded that the selected parameter range is sensible and does not qualitatively affect the conclusions on spatial attention (dynamics)[45]. Using this approach we identified 17,696 attention saccades per participant (median; range 12,377 to 28,909). We further tracked first-order sequences: Does an attention saccade focus on the same stimulus as the previous one ("stay", refocus) or shift between alternatives ("switch", reallocate). These sequences appear to be related to distinct attention functions and neuronal correlates[45].

Attention-related high-amplitude event dynamics. To assess the neuronal activity related to attention reallocation and refocus we computed the average event coincidence rate and amplitude coupling dynamics between 0.3 seconds before and after each attention reallocation/refocus. Importantly, we matched the included switch and stay by trial timing because the trial dynamics between both types vary[45]. Thus, we effectively included around 5,500 saccades per type and participant (median = 5,627, range = 3,824–10,771). We statistically tested neuronal activity between attention types, i.e., switch versus stay, applying paired t-tests of the attention-averaged activity for each sample within the attention-triggered time window (n_{sample} = 241). We applied false-discovery rate correction (FDR[57]) within each window. For analyses summarizing the activity

directly at the events (for example Fig. 3) we first averaged the data between -0.05–0.05 seconds (relative to the event) before we conducted paired t-tests on the time-averaged activity. For visualization we smoothed the peri-event activity by a 0.025s boxcar kernel.

Data Availability

The processed data generated in this study will be made publicly available upon publication.

Code Availability

The code for reproducing the main results and figures will be made publicly available upon publication.

Acknowledgements

This work was supported by grants from the European Research Council, project INFOSAMPLE, ERC-2018-StG-802905 (awarded to K.T.), and project cICMs, ERC-2022-AdG-101097402 (awarded to A.K.E.). Views and opinions expressed in this paper are those of the authors only and do not necessarily reflect those of the European Union or the European Research Council. Neither the European Union nor the granting authority can be held responsible for them.

Author Contributions

M.S., K.T. and Y.C. contributed to the experimental protocol. M.S. and Y.C. collected the data. M.S. conceptualized the functional coupling analysis. M.S. & Y.C. did the formal data analysis and M.S. visualized the results. M.S., T.H.D. & A.K.E. wrote the initial draft, all authors contributed to editing the manuscript.

Declaration of Competing Interests

The authors declare no competing interests.

References

1. Buzsáki, G. & Draguhn, A. Neuronal Oscillations in Cortical Networks. *Science* **304**, 1926–1929 (2004).
2. Sabri, E. & Batista-Brito, R. Isolating single cycles of neural oscillations in population spiking. *PLOS Computational Biology* **21**, e1013084 (2025).
3. Engel, A. K., Gerloff, C., Hilgetag, C. C. & Nolte, G. Intrinsic coupling modes: multiscale interactions in ongoing brain activity. *Neuron* **80**, 867–886 (2013).
4. Engel, A. K. & Gerloff, C. Dynamic functional connectivity: causative or epiphenomenal? *Trends in Cognitive Sciences* **26**, 1020–1022 (2022).
5. Fries, P. Rhythms for Cognition: Communication through Coherence. *Neuron* **88**, 220–235 (2015).
6. Akam, T. E. & Kullmann, D. M. Efficient 'communication through coherence' requires oscillations structured to minimize interference between signals. *PLoS Comput. Biol.* **8**, e1002760 (2012).
7. Siegel, M., Donner, T. H. & Engel, A. K. Spectral fingerprints of large-scale neuronal interactions. *Nat. Rev. Neurosci.* **13**, 121–134 (2012).
8. Siems, M. & Siegel, M. Dissociated neuronal phase- and amplitude-coupling patterns in the human brain. *NeuroImage* 116538 (2020) doi:10.1016/j.neuroimage.2020.116538.
9. Vinck, M. *et al.* Principles of large-scale neural interactions. *Neuron* **111**, 987–1002 (2023).
10. Womelsdorf, T. *et al.* Modulation of Neuronal Interactions Through Neuronal Synchronization. *Science* **316**, 1609–1612 (2007).
11. Hipp, J. F., Hawellek, D. J., Corbetta, M., Siegel, M. & Engel, A. K. Large-scale cortical correlation structure of spontaneous oscillatory activity. *Nat. Neurosci.* **15**, 884–890 (2012).

12. Buschman, T. J. & Miller, E. K. Top-Down Versus Bottom-Up Control of Attention in the Prefrontal and Posterior Parietal Cortices. *Science* **315**, 1860–1862 (2007).

13. Rohenkohl, G., Bosman, C. A. & Fries, P. Gamma synchronization between V1 and V4 improves behavioral performance. *Neuron* **100**, 953–963 (2018).

14. Womelsdorf, T. & Fries, P. The role of neuronal synchronization in selective attention. *Current opinion in neurobiology* **17**, 154–160 (2007).

15. Fell, J. & Axmacher, N. The role of phase synchronization in memory processes. *Nat Rev Neurosci* **12**, 105–118 (2011).

16. Buschman, T. J., Denovellis, E. L., Diogo, C., Bullock, D. & Miller, E. K. Synchronous Oscillatory Neural Ensembles for Rules in the Prefrontal Cortex. *Neuron* **76**, 838–846 (2012).

17. Boroujeni, K. B. & Womelsdorf, T. Routing states transition during oscillatory bursts and attentional selection. *Neuron* **111**, 2929–2944 (2023).

18. Hipp, J. F., Engel, A. K. & Siegel, M. Oscillatory synchronization in large-scale cortical networks predicts perception. *Neuron* **69**, 387–396 (2011).

19. Helfrich, R. F. *et al.* Spectral fingerprints of large-scale cortical dynamics during ambiguous motion perception. *Human Brain Mapping* **37**, 4099–4111 (2016).

20. Galindo-Leon, E. E. *et al.* Dynamic changes in large-scale functional connectivity prior to stimulation determine performance in a multisensory task. *Frontiers in Systems Neuroscience* **19**, 1524547 (2025).

21. Schölvinck, M. L., Leopold, D. A., Brookes, M. J. & Khader, P. H. The contribution of electrophysiology to functional connectivity mapping. *Neuroimage* **80**, 297–306 (2013).

22. Donner, T. H., Siegel, M., Fries, P. & Engel, A. K. Buildup of Choice-Predictive Activity in Human Motor Cortex during Perceptual Decision Making. *Current Biology* **19**, 1581–1585 (2009).

23. Mostame, P. & Sadaghiani, S. Phase-and amplitude-coupling are tied by an intrinsic spatial organization but show divergent stimulus-related changes. NeuroImage, 219, Article 117051. (2020).

24. Galindo-Leon, E. E. *et al.* Context-specific modulation of intrinsic coupling modes shapes multisensory processing. *Science advances* **5**, eaar7633 (2019).

25. Siems, M., Tünnerhoff, J., Ziemann, U. & Siegel, M. Multistage classification identifies altered cortical phase- and amplitude-coupling in Multiple Sclerosis. *NeuroImage* **264**, 119752 (2022).

26. Cabral, J. *et al.* Exploring mechanisms of spontaneous functional connectivity in MEG: How delayed network interactions lead to structured amplitude envelopes of band-pass filtered oscillations. *NeuroImage* **90**, 423–435 (2014).

27. Leopold, D. A., Murayama, Y. & Logothetis, N. K. Very slow activity fluctuations in monkey visual cortex: implications for functional brain imaging. *Cereb. Cortex* **13**, 422–433 (2003).

28. Pfeffer, T. *et al.* Circuit mechanisms for the chemical modulation of cortex-wide network interactions and behavioral variability. *Science Advances* **7**, eabf5620 (2021).

29. Hindriks, R. & Tewarie, P. K. Dissociation between phase and power correlation networks in the human brain is driven by co-occurrent bursts. *Communications biology* **6**, 286 (2023).

30. Tewarie, P. *et al.* Tracking dynamic brain networks using high temporal resolution MEG measures of functional connectivity. *NeuroImage* **200**, 38–50 (2019).

31. Seedat, Z. A. *et al.* The role of transient spectral 'bursts' in functional connectivity: A magnetoencephalography study. *NeuroImage* **209**, 116537 (2020).

32. Lundqvist, M., Miller, E. K., Nordmark, J., Liljefors, J. & Herman, P. Beta: bursts of cognition. *Trends in cognitive sciences* (2024).

33. Tal, I., Neymotin, S., Bickel, S., Lakatos, P. & Schroeder, C. E. Oscillatory bursting as a mechanism for temporal coupling and information coding. *Frontiers in Computational Neuroscience* **14**, 82 (2020).

34. van Ede, F., Quinn, A. J., Woolrich, M. W. & Nobre, A. C. Neural oscillations: sustained rhythms or transient burst-events? *Trends in neurosciences* **41**, 415–417 (2018).

35. Banaie Boroujeni, K. *et al.* Fast Attentional Information Routing via High-Frequency Bursts in the Human Brain. *bioRxiv* 2024–09 (2024).

36. Kosciessa, J. Q., Grandy, T. H., Garrett, D. D. & Werkle-Bergner, M. Single-trial characterization of neural rhythms: Potential and challenges. *NeuroImage* **206**, 116331 (2020).

37. Myrov, V. *et al.* Rhythmicity of neuronal oscillations delineates their cortical and spectral architecture. *Communications biology* **7**, 405 (2024).

38. Schmidt, R., Rose, J. & Muralidharan, V. Transient oscillations as computations for cognition: Analysis, modeling and function. *Current Opinion in Neurobiology* **83**, 102796 (2023).

39. Buzsáki, G., Anastassiou, C. A. & Koch, C. The origin of extracellular fields and currents—EEG, ECoG, LFP and spikes. *Nature reviews neuroscience* **13**, 407–420 (2012).

40. Donoghue, T. *et al.* Parameterizing neural power spectra into periodic and aperiodic components. *Nature neuroscience* **23**, 1655–1665 (2020).

41. Voytek, B. & Knight, R. T. Dynamic network communication as a unifying neural basis for cognition, development, aging, and disease. *Biol. Psychiatry* **77**, 1089–1097 (2015).

42. Arazi, A., Toso, A., Grent-‘t-Jong, T., Uhlhaas, P. J. & Donner, T. H. Large-scale maps of altered cortical dynamics in early-stage psychosis are related to GABAergic and glutamatergic neurotransmission. *Science Advances* **11**, eads0400 (2025).

43. Vinck, M., Uran, C., Dowdall, J. R., Rummell, B. & Canales-Johnson, A. Large-scale interactions in predictive processing: oscillatory versus transient dynamics. *Trends in cognitive sciences* (2024).

44. Ibarra Chaoul, A. & Siegel, M. Cortical correlation structure of aperiodic neuronal population activity. *NeuroImage* **245**, 118672 (2021).

45. Siems, M., Cao, Y., Tohidi-Moghaddam, M., Donner, T. H. & Tsetsos, K. Rhythmic sampling of multiple decision alternatives in the human brain. *bioRxiv* 2023.12.08.570734 (2025) doi:10.1101/2023.12.08.570734.

46. Capilla, A. *et al.* The natural frequencies of the resting human brain: An MEG-based atlas. *NeuroImage* **258**, 119373 (2022).

47. Fiebelkorn, I. C. & Kastner, S. Functional specialization in the attention network. *Annual review of psychology* **71**, 221–249 (2020).

48. Gaillard, C. *et al.* Prefrontal attentional saccades explore space rhythmically. *Nat Commun* **11**, 925 (2020).

49. Fries, P. Rhythmic attentional scanning. *Neuron* **111**, 954–970 (2023).

50. Okazawa, G. & Kiani, R. Neural mechanisms that make perceptual decisions flexible. *Annual review of physiology* **85**, 191–215 (2023).

51. Heekeren, H. R., Marrett, S. & Ungerleider, L. G. The neural systems that mediate human perceptual decision making. *Nature reviews neuroscience* **9**, 467–479 (2008).

52. Wu, L., Liu, T. & Wang, J. Improving the effect of transcranial alternating current stimulation (tACS): A systematic review. *Frontiers in Human Neuroscience* **15**, 652393 (2021).

53. Siems, M., Pape, A.-A., Hipp, J. F. & Siegel, M. Measuring the cortical correlation structure of spontaneous oscillatory activity with EEG and MEG. *Neuroimage* **129**, 345–355 (2016).

54. Hipp, J. F. & Siegel, M. Dissociating neuronal gamma-band activity from cranial and ocular muscle activity in EEG. *Front Hum Neurosci* **7**, 338 (2013).

55. Oostenveld, R., Fries, P., Maris, E. & Schoffelen, J.-M. FieldTrip: open source software for advanced analysis of MEG, EEG, and invasive electrophysiological data. *Computational intelligence and neuroscience* **2011**, 156869 (2011).

56. Cook, A. J., Im, H. Y. & Giaschi, D. E. Large-scale functional networks underlying visual attention. *Neuroscience & Biobehavioral Reviews* **173**, 106165 (2025).

57. Benjamini, Y. & Hochberg, Y. Controlling the False Discovery Rate: A Practical and Powerful Approach to Multiple Testing. *Journal of the Royal Statistical Society. Series B (Methodological)* **57**, 289–300 (1995).